Appl. Phys. B 73, 345–353 (2001)
DOI: 10.1007/s003400100636

Applied Physics B
Lasers and Optics

P.D. TOWNSEND[1,✉]
R. BROOKS[1]
D.E. HOLE[1]
Z. WU[1,2]
A. TURKLER[1,3]
N. CAN[3]
A. SUAREZ-GARCIA[4]
J. GONZALO[4]

Luminescence from copper nanoparticles

[1] Engineering and Information Technology Department, University of Sussex, Brighton BN1 9QH, United Kingdom
[2] Analytical and Testing Center, Beijing Normal University, Beijing 100875, China
[3] Physics Department, Faculty of Arts and Sciences, Celal Bayar University, Manisa, Turkey
[4] Instituto de Optica, CSIC, Serrano 121, 28006 Madrid, Spain

Received: 29 June 2001
Published online: 10 October 2001 •

ABSTRACT The presence of copper nanoparticles in alumina and silica modifies their luminescence, and the changes in spectra are influenced by variations in the nanoparticle size distributions. Luminescence signals are sensitive to the total defect population. Thus the luminescence not only reflects changes caused by thermal annealing, which can modify both intrinsic defects and the copper nanoparticles, but also responds to the method of preparation of thin film layers. Copper nanoparticle influence on luminescence is reported both for ion-implanted bulk silica and for copper in pulsed laser deposition within alumina. Luminescence thus potentially offers a non-destructive monitor of the layer quality, reproducibility and growth conditions, as well as the state and size of the copper nanoparticles.

PACS 81.05.Y; 68.55.L; 78.60.H

1 Introduction

The intense interest in metallic nanoparticles embedded in insulating host materials stems in part from the wide range of possible applications and in part from the progress in theoretical modelling of their properties. Existing optical applications have included examples as ancient as the fabrication of ruby glass [1] to diverse modern examples such as the fabrication of car mirrors [2], mirror front sunglasses [3] and high extinction polarisers [4]. More recently, emphasis has moved toward the use of non-linear optical properties, which exploit changes in third-order susceptibility and consequent modifications of refractive index and absorption that operate on the sub-picosecond timescale (i.e. for devices with rapid optical switches). Theoretically, the description of the optical resonances is well advanced [5], but experimentally there are problems since the host lattice is considerably disturbed under most methods of preparation. In practice, the nanoparticles are often formed in a variety of sizes with a distribution which varies with depth in the sample. The problem is unavoidable in the original fabrication step when using surface modification by metallic ion implantation [6–8] but to some extent may be subsequently modified by pulsed laser or other thermal treatments [9, 10]. Alternative methods, such as pulsed laser deposition, can control the depth at which nanoparticles are formed, but still suffer from problems of large-scale uniformity and a range of particle sizes [11–13]. Similarly, sol-gel routes include a range of particle sizes [14]. Note that interest in the topic includes both the "bulk" material discussed here and the non-linear optical responses of nanoparticles on, or very close to, the surface [15].

Analysis of the optical responses as a function of particle size requires an accurate determination of the size distribution, and whilst this is achievable by sectioning and transmission electron microscopy (TEM), such a technique is destructive. Therefore, there is the need to find a sensitive and simple technique, which can ideally be both correlated to the optical responses and simultaneously provide a non-destructive monitor of changes within the sample, including the particle size. A potential candidate for this role is the recording of luminescence responses. The strength, and weakness, of luminescence measurements is their extreme sensitivity to defects and their interactions, hence many signals will arise from sites that are not central to the main objective. Overall, the host material will have intrinsic luminescence signals, for example from relaxation of excitons and electron-hole pairs, as well as a wide range of site-specific signals from both intrinsic and extrinsic defect sites in the lattice structure (or glass network). Addition of impurity ions in the concentrations needed to form nanoparticles will modify many of these host responses in terms of wavelength, quantum efficiency, relative intensities of component luminescence bands, temperature dependencies and lifetimes. In addition, there may be totally new signals originating at the metal ion sites and variations of these signals as a function of particle size. With such a plethora of possible interactions it is highly unlikely that it will be possible to identify the precise origin of more than a few of the various signals. Nevertheless, the high sensitivity of luminescence detection, combined with spectral and lifetime information, provide monitors of the state of the material which are valuable in selecting fabrication parameters and monitoring consistency in production. Ideally such luminescence responses may be correlated with TEM data and optical non-linear responses.

✉ Fax: 44-1273/678-073, E-mail: p.d.townsend@sussex.ac.uk

In general, luminescence can be stimulated by various energy sources such as optical photons (PL), X-rays (RL), electrons (CL) or ion beams (IBL). Luminescence linked to nanoparticles has received very limited study. Examples so far have included some biological sensors [16, 17], silicon and rare earth nanoparticles for laser and light sources [18–23] and examples with II–VI compounds [15, 16]. In the present work, luminescence has been recorded from copper-implanted silica glass and nanocomposite Cu:Al_2O_3 formed by pulsed laser deposition (PLD) of copper within a layer of alumina. In both cases the modified materials are of a thickness well below a micron, so the near-surface techniques of CL and IBL have been employed. PL is equally appropriate, but has not yet been used in detail for these samples. RL was not considered since it would excite a large volume of material and hence near-surface effects would be disguised by the bulk signals.

2 Experimental details

The ion implantations were made with Cu at a beam energy of 50 keV and at a dose of up to 4×10^{16} ions/cm^2. The substrate material in these cases was silica. Previous experience has shown that for reproducible optical signals from the copper nanoparticles, in terms of optical reflectivity, transmission and $\chi^{(3)}$ non-linear effects, it was essential to control the substrate temperature to within 5 °C and to maintain a uniform dose rate (i.e. current density) throughout the implant. In terms of optical reflectivity, all the samples monitored here were uniform and identical.

Nanocomposite Cu:Al_2O_3 thin films consisting of a single layer of Cu nanoparticles (NPs) embedded in an Al_2O_3 matrix have been prepared by sequential pulsed laser deposition (PLD) using an ArF excimer laser ($\lambda = 193$ nm, $\tau =$ 20 ns FWHM) operating at 20 Hz. The laser beam was sequentially focused on the surface of high purity Al_2O_3 and Cu targets at an angle of incidence of 45°, giving an average energy density of approximately 2 J/cm^2, a value large enough to ablate both targets. The targets were mounted in a computer-controlled holder that provided both the continuous rotation and the sequential ablation of the targets. The nanocomposite films were grown at room temperature on Si substrates, which had a 2.5-μm-thick, thermally grown, oxide layer. This silica layer was 32 mm away from the target surface. Earlier works have shown that the presence of an Ar environment during the synthesis of the Cu NPs modifies their in-plane shape [13, 24]. Thus, either a base pressure of 1.3×10^{-6} mbar (vacuum) or Ar pressures of 1.3×10^{-4} and 1.3×10^{-1} mbar have been considered in the present work to produce the Cu NPs, whereas the Al_2O_3 matrix was always grown in vacuum in order maintain its structural characteristics. Such a variety of growth conditions have been used, since one objective of the luminescence study was to attempt to recognise differences or characteristic features of the PLD operating conditions.

The films were grown in a sandwich structure of (Al_2O_3–Cu NPs–Al_2O_3); this offered the NPs protection against oxidation. The thicknesses of the first and last Al_2O_3 layers were 10 and 390 nm, respectively, and the effective thickness of Cu (if it were continuous) was 1 nm. This metal content was selected since it has earlier been reported that it leads to the formation of isolated Cu NPs [13, 24]. The use of an Ar environment decreases the deposition rate of the metal layer as compared to that in vacuum and thus, the number of laser pulses on the Cu target was increased accordingly to achieve films with similar Cu content. Table 1 summarizes the experimental conditions used to produce the Cu:Al_2O_3 films. Further details on the synthesis procedure of the nanocomposite films can be found elsewhere [13, 24].

Ar pressure (mbar)	No. of Cu layers	No. of pulses in Cu	Cu areal density ($\times 10^{15}$ at./cm^2)	Thickness (nm)
1.3×10^{-6}	0			400
1.3×10^{-6}	1	200	4.0	400
1.3×10^{-4}	1	200		400
1.3×10^{-1}	1	780		400

TABLE 1 Experimental parameters used to grow the Cu:Al_2O_3 nanocomposite films; Cu areal density, as determined from RBS, and total thickness of the films

The Cu content in some films was determined by Rutherford backscattering spectrometry (RBS) using a 2.0 MeV $^4He^+$ beam. The backscattered particles were detected at an angle of 150° and the experimental spectra were simulated by using the RUMP program [25].

Luminescence was excited either by electrons or ion beams. For the CL (cathodoluminescence) measurements, the beam energy was chosen between 10 and 20 keV and a low current of typically 20 nA was defocused over about 1 sq cm. Sinusoidal beam modulation with lock-in amplifier detection was used in the range from 9 Hz to 20 kHz. Measurements were made at temperatures from ambient down to approximately 25 K. Ion beam luminescence data shown here primarily used a helium beam at 1 MeV with a current density of approximately 2 μA/cm^2.

The lowest energy electrons primarily deposit energy only in the Cu nanoparticle layer in the case of PLD samples, or, for the ion implanted silica samples, in the implant region. Higher electron energies penetrate into the underlying layers. Hence signals are more difficult to interpret, since they combine data from at least two zones. For all the IBL data, the excitation range extends far beyond the implant or nanoparticle layer. However, a bonus of the IBL compared with the CL case is that the rate of excitation within the zone is nearly constant, so effects of surface states are less dominant.

In both cases the luminescence intensities of the detected signals were corrected for the wavelength response of the respective spectrometers and detectors used. For attempts at analysis into component emission bands, the signals were transformed from the recorded wavelength data of $I(\lambda)\,\mathrm{d}\lambda$ versus λ into energy plots of $I(E)\,\mathrm{d}E$ versus E. Analysis into a set of overlapping Gaussian emission bands was then attempted. Whilst the analysis clearly showed the presence of numerous features, there was still uncertainty associated with the true number of component features, since, as will be shown, the spectra included differently resolved components for different CL modulation frequencies and temperatures, and these changed on annealing the sample at different temperatures. In the case of the PLD films, the analysis was not feasible since there was a strong thin film interference effect apparent from the use of the reflecting silicon substrate.

3 Results and comments for copper-implanted silica

In the simplest situation it is assumed that copper implantation of silica glass will have two main effects. The first is to introduce copper and the other to create defects in the host silica lattice. Annealing of the samples will modify both types of defect site and, in general, the simpler intrinsic defects will be removed by higher temperature anneals. The immediate initial effects of the copper ion beam implantation are seen in Fig. 1 for CL measurements. At a modulation frequency of just 9 Hz (i.e. effectively continuous ~ dc excitation) the main signal peaks near 440 nm in both cases, but there are poorly resolved additional features in the tails of the central region. Although at first sight the data obtained at higher modulation frequencies are similar, Fig. 1b reveals that quite different component bands are dominant. For the modulation frequency of 900 Hz (i.e. signals with lifetimes much longer than a few milliseconds are rejected) the main peak is near 400 nm and this band was only a shoulder on the 9 Hz data. Several other peaks are also resolved for the Cu-implanted material. Rather than view just the original wavelength signals, the data should be transformed into energy plots. Figure 2 shows a set of data which emphasise the importance of longer wavelength signals and allow attempts at deconvolution of the spectra into Gaussian-shaped component bands. Such analyses must be viewed with caution, but nevertheless there are clear differences between the original silica and the copper-implanted material in terms of relative peak intensity and band position. There are apparent peak movements and changes in the relative intensities of the component bands. Some of the similarities may result from electrons exciting deeper "bulk" silica regions in both the original and Cu-implanted cases.

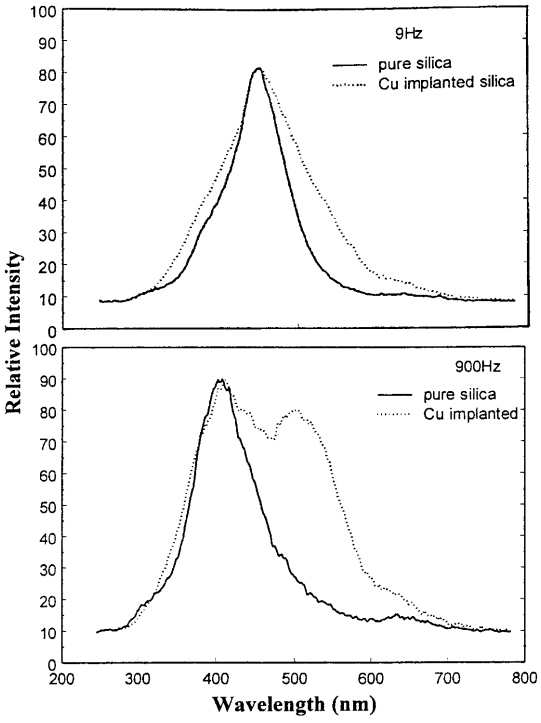

FIGURE 1 Comparisons of cathodoluminescence for pure and Cu-implanted silica recorded at 9 and 900 Hz. Note the dominant peaks differ in the two cases

Figure 3 presents further data for CL taken at 900 Hz, following furnace anneals at 200 and 500 °C. In these cases, the original silica signals are closely similar (albeit with minor differences in the attempts at computer analysis). The copper implant signals change significantly in terms of their com-

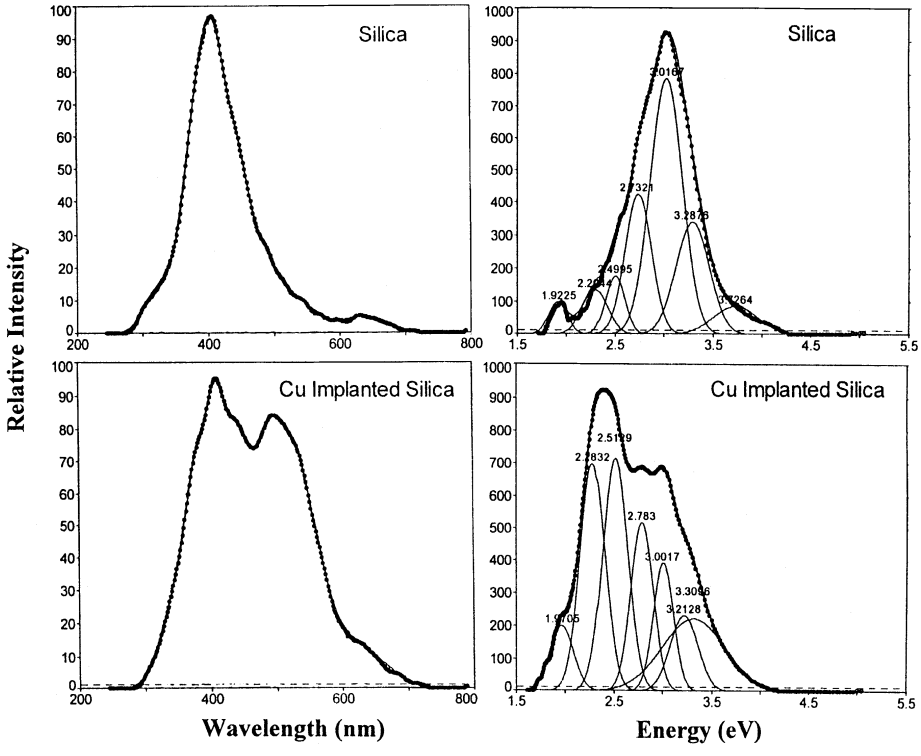

FIGURE 2 Cathodoluminescence of pure silica and Cu-implanted silica recorded at room temperature and at 900 Hz. The left-hand diagrams are as recorded in wavelength dispersed data, and the right-hand diagrams show how these transform into energy plots

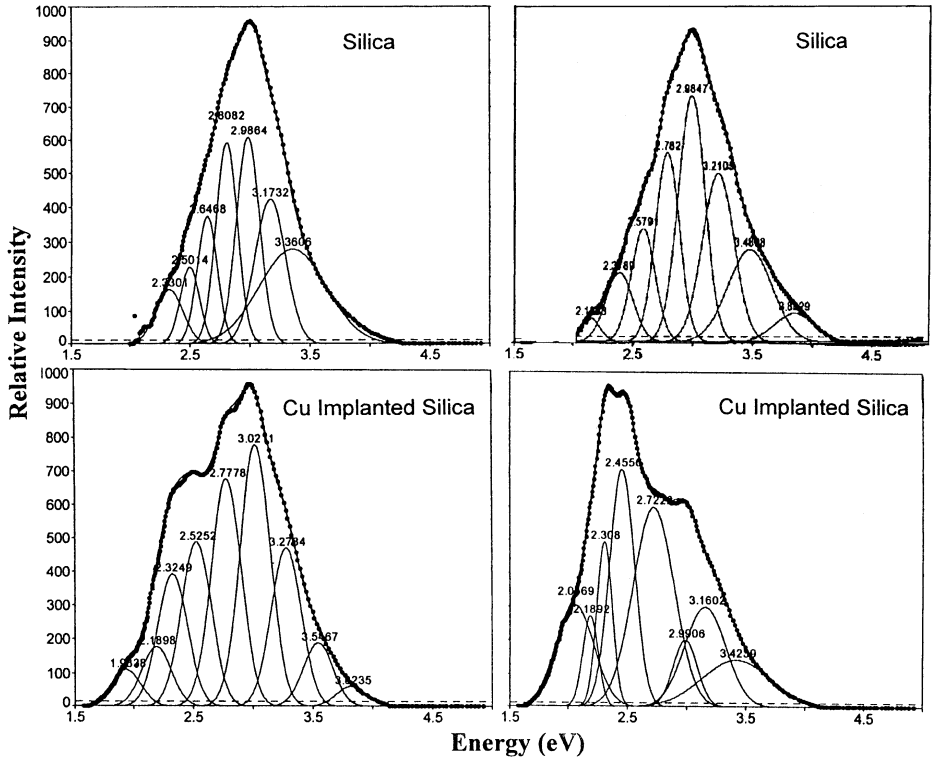

FIGURE 3 Cathodoluminescence of pure silica and Cu-implanted silica recorded at room temperature and 900 Hz. The left-hand diagrams were taken after 200 °C and the right-hand diagrams after 500 °C anneals

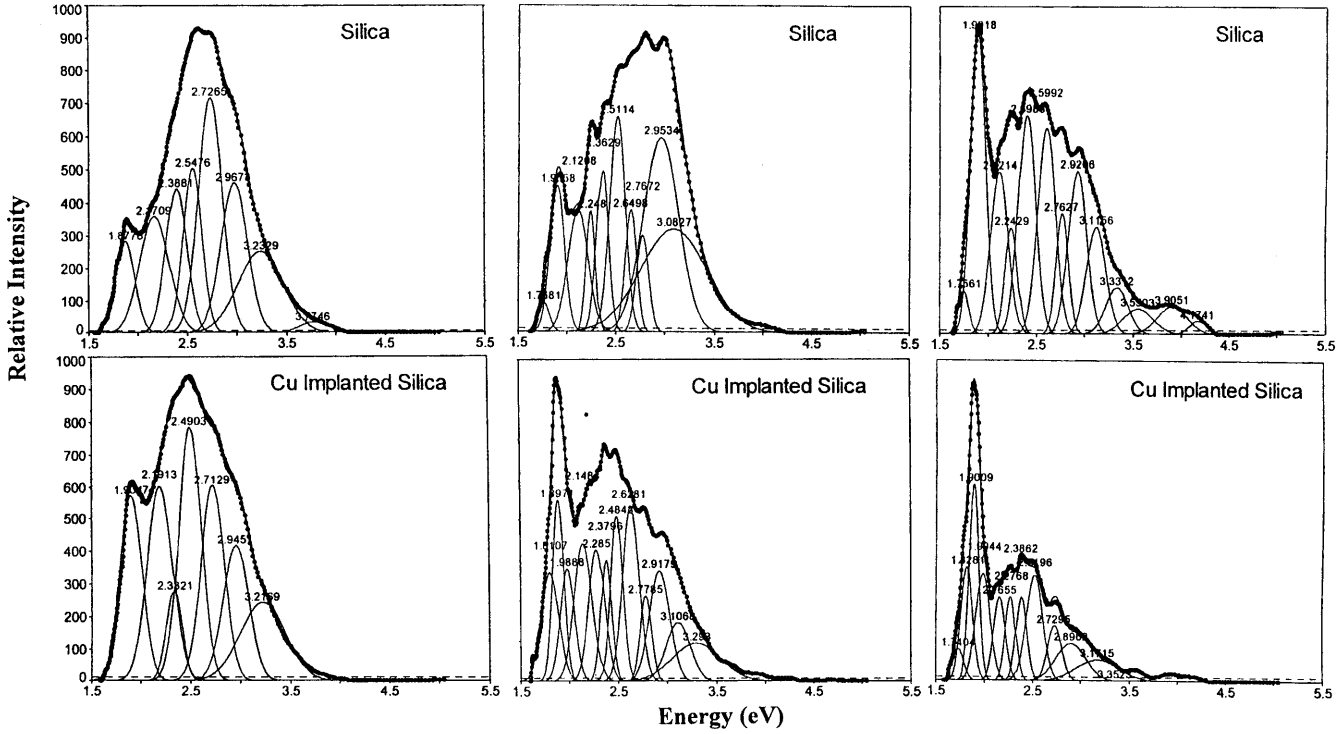

FIGURE 4 Cathodoluminescence of pure silica and Cu-implanted silica taken at 25 K. From left to right the modulation frequencies were 90, 900 and 9000 Hz. Attempts at Gaussian band analyses are shown

ponent features, with strong emphasis on the lower energy peaks near 2.4 eV, which have increased from the original data after the 200 °C anneal, and grow even more after the 500 °C anneal.

In addition to resolution of component bands by studying lifetime components (via the use of different modulation frequencies, with lock-in amplifier detection) there are further differences which can be viewed by changing the measurement temperature. Figure 4 combines examples of such analyses by showing normalised data for the original (unannealed) silica and copper-implanted silica taken at 25 K for three modulation frequencies. Note that in absolute terms the

intensity of the higher frequency signals is less. Signals obtained at higher modulation frequencies are weaker, since long-lived components are successively rejected. Also note that the copper-implanted samples are brighter, typically by a factor of 5 to 10 times, depending on the copper ion dose and thermal processing. Whilst the data show that there are many more component bands apparent from the low-temperature data, there is still a broad trend that the copper shifts the strong blue/green emission from approximately 2.75 towards 2.5 eV. The feature near 1.9 eV is presumably related to the silica, since it appears strongly in each type of sample.

4 Discussion of CL from copper-implanted silica

The most striking feature of these analyses is the number of different luminescence sites which exist, even in the original silica. The number of resolved components is emphasised at the higher modulation frequencies of the CL and at low temperature. Note that low-temperature CL may include signals from additional sites. The analysis attempts assume Gaussian-shaped energy bands and, although such analyses are often suspect in detail, the signal to noise quality of the original data is excellent and reproducible. Therefore the process suggests that perhaps as many as 10 different luminescence centres contribute to the overall signal. It must also be recognised that CL is not a passive probe of the structure, but the high energy electrons will both stimulate existing defect sites, alter the charge population of sites, and for most glasses, including silica, introduce new intrinsic damage and density changes. For silica this long-term damage accrues relatively slowly and at the electron doses used here the spectra were not obviously changing with time. Hence CL induced changes are only a minor factor in the current analysis of the silica samples.

Implantation of copper clearly shifts the peak position of the dominant peaks to provide strong signals near 2.5 eV (i.e. $\sim$ 500 nm). More detailed examination suggests the copper has raised, or introduced, the importance of shorter wavelength bands near 3.2 eV. Broadly these trends were apparent even in the simplest data set of Fig. 1. The annealing data of Fig. 3 indicates that more copper related bands appear in the 2.5 eV region as the result of higher temperature treatments. The same temperature cycling modifies the size of copper nanoparticles. Broadly, one may expect association and growth of particles at lower temperatures and dissolution at high temperatures, but final nanoparticle sizes are strongly influenced by the sample cooling rate, since regrowth of dissolved particles will occur during slow cooling.

In the present case, the first assumption is that the higher temperatures have resulted in more isolated copper ions and hence their presence increases the luminescence intensity from copper-related emission bands. There is however always a doubt in such situations as to whether the metal ion itself is at the origin of the luminescence, or whether the presence of the ion stabilises an intrinsic type defect which is therefore more intense in the doped material. (The latter situation is well documented for another oxide example of tin-doped float glass [26].) In the present silica case, the peak positions and the number of components seem to change with annealing, so the more probable factor is the increase and change in the distribution of associated copper ions. This is convenient if the luminescence is to be used as a monitor of the nanoparticle size distribution. To exploit correlation between luminescence spectra and size distributions, the latter need to be ascertained from TEM data. Unfortunately TEM will not respond to copper ions which are isolated or in very small clusters, and these are precisely the ions which are most likely to dominate the luminescence responses. Nevertheless, the luminescence has shown that it is sensitive to the presence of the copper implants and the nanoparticle size distribution, and consequently it can offer a sensitive, albeit empirical, monitor of the situation.

5 Results and comments on PLD alumina

Pulsed laser deposition is a flexible and powerful technique for the deposition of thin films, that in addition allows the possibility of doping in precise layers. In recent experiments this has been exploited to introduce copper nanoparticles into alumina layers to give extremely high performance $\chi^{(3)}$ non-linear responses. Nevertheless, the uniformity of the deposition is limited over large areas and the composition. The density and structure of the layer is sensitive to numerous parameters of the PLD process, for example the background gas composition and pressure. Consequently, luminescence has been used here as a probe to assess if the signals can offer information on the intrinsic defects and/or dopants in the layer. Additionally, the luminescence can be used to monitor layer reproducibility at the important level of the imperfections, rather than merely at the level of composition.

In order to separate signals from the PLD film and from the underlying silica layer, the CL experiments were made with energies as low as 6 keV. Higher energies of up to 20 keV can stimulate signals from a combination of the alumina PLD film and the silica substrate. From both silica and alumina, the "normal" CL emission is in the range 400 to 500 nm. The similarity is probably due to comparable excited electron-hole relaxation and emission steps in the materials of comparable dielectric constant.

Figure 5 compares the 9 Hz and 9 kHz data taken using a 10 kV CL beam on the alumina PLD films with and without a single layer of copper nanoparticles. The measurement temperature of 56 K emphasises the longer wavelength features (i.e. near 2 eV). As with the silica example of Fig. 1, it is clear that the copper has shifted the peak to longer wavelengths. The alumina/Cu samples also have a stronger signal at longer wavelengths, although at 9 kHz the signal exists even for "undoped" alumina. The undoped layers have very similar spectra from 9 to 900 Hz, but greater differences appear at higher modulation frequencies, and also when the Cu layer is included.

Despite the strength of the signals, they have an oscillatory component which modulates the signal as a function of wavelength. This is mainly an artefact of excitation of a thin film layer on top of the silica waveguide and silicon substrate, since the refractive index differences at the interfaces introduce sets of thin film interference characteristics, which are superposed on the emission spectra. Most obvious are the thin film effects from reflection at the underlying silicon. This is an

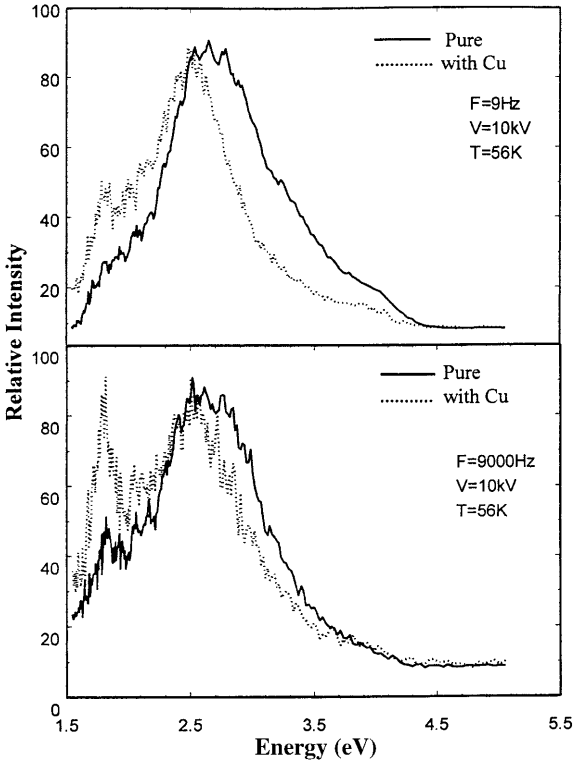

FIGURE 5 Cathodoluminescence of PLD alumina on a silica/silicon substrate at 56 K using 10 keV electrons at 9 Hz and 9 kHz modulation. The data for a copper-doped film are *dotted*

unfortunate situation since it is impossible to make any spectral deconvolution, as was presented for the ion-implanted silica. With this caveat, Fig. 6 presents data for three electron energies into a pair of samples with and without a copper nanoparticle layer. The 10 keV electrons primarily deposit energy near the upper surface of the alumina film, whereas the 15 keV electrons penetrate through the Cu layer quite efficiently and 20 keV electrons will generate some luminescence signal from the silica underlayer. Since silica tends to be a much brighter CL material than alumina, even the small energy deposition into the silica influences the overall spectra. The only clear conclusion is that the copper has a major effect on the spectra, both in intensity and energy components, even though it represents a very small fraction of the total electron range.

Ion beam luminescence of the samples uniformly excites the alumina layer but penetrates deeply into the silica and so has short wavelength spectra dominated by the silica underlayer. Nevertheless, Fig. 7 shows distinct differences between samples with and without copper in the PLD alumina. Features to note are that the multilayer interference features are very cleanly defined and the copper has an intense signal at the longer wavelengths. There is also a very strong emission from the copper doped material near 250 nm, which was indicated, but at the limit of measurement for the CL analysis for 9 Hz detection. These copper signals appear therefore to be emission features with very long lifetimes, hence they are seen by the DC IBL but virtually rejected even at 9 Hz in the CL.

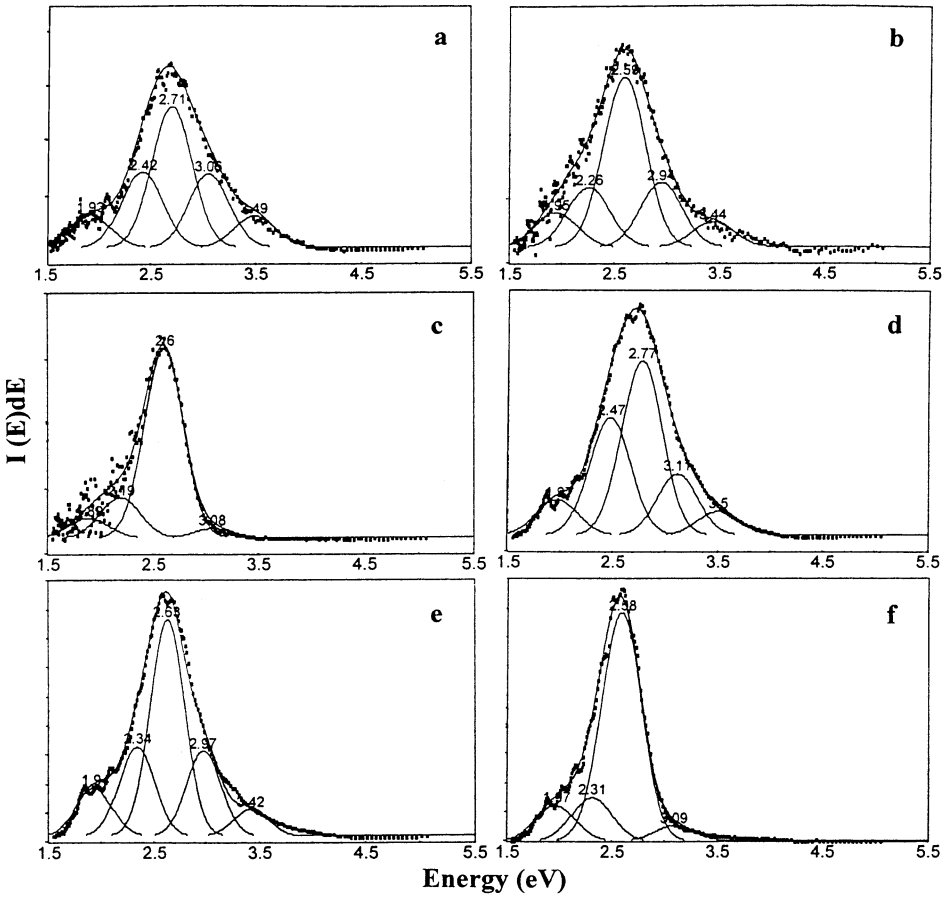

FIGURE 6 Cathodoluminescence of PLD alumina on a silica/silicon substrate for three electron energies and 9 Hz modulation. The left-hand diagrams are for undoped alumina, and the right-hand diagrams include a copper layer. Energies are 10 keV (**a** and **b**), 15 keV (**c** and **d**), and 20 keV (**e** and **f**)

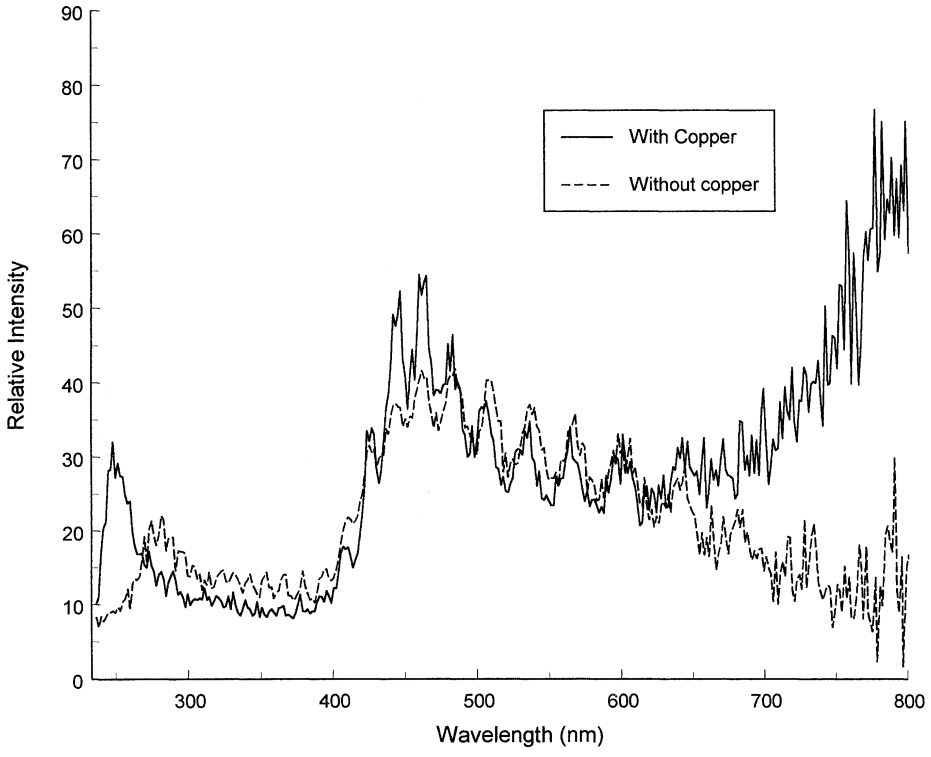

FIGURE 7 Ion beam luminescence of PLD alumina on a silica/silicon substrate contrasting the signals from an undoped film with one containing a Cu layer

Figure 8 offers IBL data for three different thicknesses of the PLD layer. The thin film interference feature is pronounced for the thinner layers, as are the signals near 300 nm. However, for the thickest layer the alumina thickness is comparable to that of the silica and the interference pattern shifts accordingly. More importantly, the 300 nm features are suppressed as is the overall intensity. This implies that much of the strong emission near both 300 and 500 nm has arisen from the underlayer, not the alumina.

Using luminescence as a test of changes in the background gas pressure for PLD deposition has proved informative. The data of Fig. 9 display the responses from samples of the same

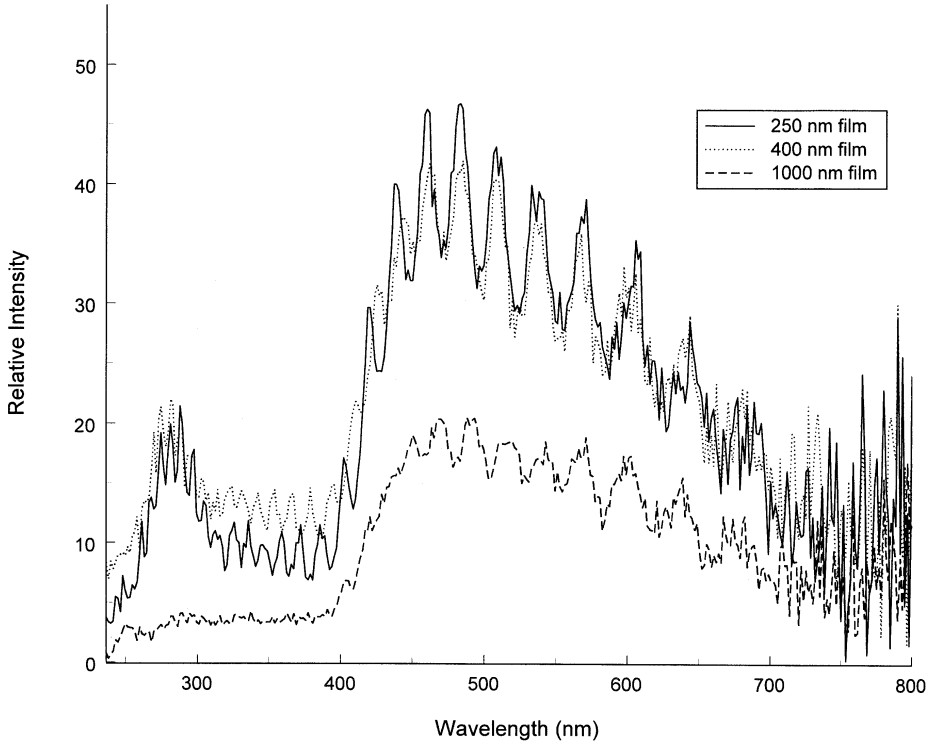

FIGURE 8 Ion beam luminescence of PLD alumina on a silica/silicon substrate for alumina films of 250, 400 and 1000 nm

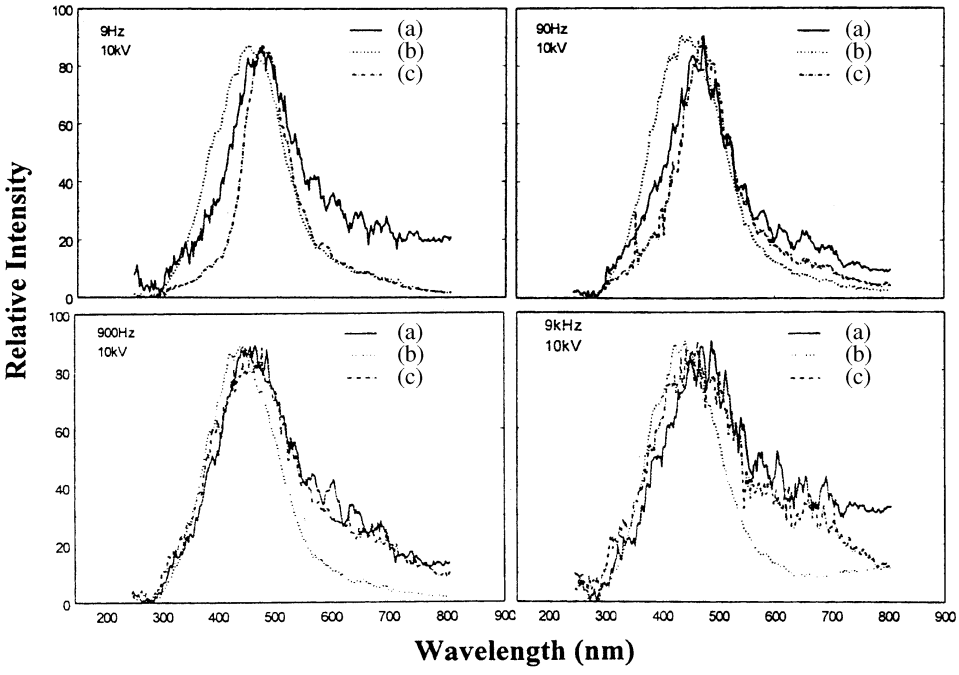

FIGURE 9 Cathodoluminescence of PLD alumina on a silica/silicon substrate using different Ar gas pressure growth conditions of (a) 1.3×10^{-6}, (b) 1.3×10^{-4}, and (c) 1.3×10^{-1} mbar. The different CL modulation frequencies of 9, 90, 900 and 9000 Hz show varying lifetime components. The data on the left are for undoped alumina and on the right are for a film including a copper layer

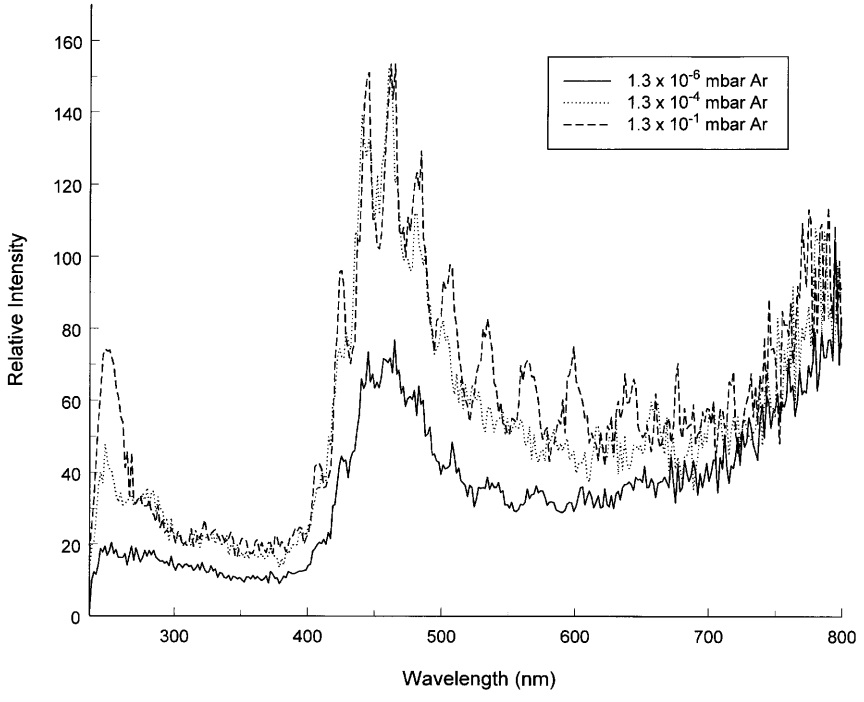

FIGURE 10 Ion beam luminescence of PLD alumina on a silica/silicon substrate using different Ar gas pressure growth conditions of 1.3×10^{-6}, 1.3×10^{-4}, and 1.3×10^{-1} mbar

thickness (400 nm of PLD alumina), formed at three different background gas pressures of argon. The brightest signals came from the lowest gas pressure when recording at 9 Hz, but at higher frequencies the intensities maximised at the 10^{-4} mbar Ar pressure. Figure 9 emphasises that the Ar pressure influences the spectra of the lifetime-resolved components and the intensity effects indicate that the fraction of the relevant defect sites differ with growth conditions.

Gas pressure also has a pronounced effect on the signals from the copper layer [13, 24] and this is easily seen in Fig. 10 for the DC IBL data. Lower pressure reduces the Cu-related signals, whereas higher argon pressures strongly enhance the alumina emission with the 250 nm feature, and the interference oscillations, rising with Ar pressure. This suggests that the argon is influencing not only the way the copper is incorporated, but is also modifying the charge state of the copper and the associated luminescent sites.

6 Conclusions

There is a clear influence on the luminescence response from the silica and alumina layers which contain copper nanoparticles. In both cases there is a shift in the peak wavelength towards longer wavelengths and strong long

wavelength emission bands in the copper samples. The example of ion-implanted silica emphasises signals are altered by thermal treatments in a furnace, and it is noted that such treatments influence the sizes of the nanoparticles. Spectral analysis and measurements at a range of temperatures indicate that the host silica doped with Cu contains at least 10 different luminescence sites. For the PLD material, the single layer of copper in alumina introduces significant luminescence features. For undoped alumina, the spectra respond differently to changes in argon pressure during PLD.

Both types of response indicate luminescence could be used as a non-destructive monitor of material quality and reproducibility of preparation procedure. Ideally, following correlation with TEM studies, the changes in signal might even be related to the nanoparticle size distribution. With at least 10 different luminescence mechanisms it is not yet possible to offer detailed models of the luminescence sites, although there is correlation with earlier signals seen in alumina and silica.

ACKNOWLEDGEMENTS We wish to thank the EPSRC, and BRITE EURAM for Contract No. BRPR-CT98-0616, Project No. BE 4427 (AMENIDAD), for financial support.

REFERENCES

1 M. Faraday: Proc. Roy. Soc. London **8**, 356 (1857)
2 P.D. Townsend, L. Massarelli: US Patent No. 07/618, 507 (1991)
3 P.D. Townsend, D. Menaguale: European Patent No. 94830012.4 (1994)
4 Polarcor^{TM}, Corning, New York.
5 C. Flytzanis, F. Hache, M.C. Klein, D. Ricard, P. Roussignol: Prog. Opt. XXIX, 321 (1991)
6 R.F. Haglund: Mat. Sci. Eng. A **253**, 275 (1998)
7 A. Meldrum, L.A. Boatner, C.W. White, R.C. Ewing: Mater. Res. Innovation **3**, 190 (2000)
8 F. Gonella: Nucl. Instrum. Meth. B **166**–**167**, 831 (2000)
9 R.A. Wood, P.D. Townsend, N.D. Skelland, D.E. Hole, J. Barton, C.N. Afonso: J. Appl. Phys. **74**, 5754 (1993)
10 P.D. Townsend, J. Olivares: Appl. Surf. Sci. **110**, 275 (1997)
11 J.M. Ballesteros, R. Serna, J. Solis, C.N. Afonso, A.K. Petford-Long, D.H. Osborne, R.F. Haglund: Appl. Phys. Lett. **71**, 2445 (1997)
12 R. Serna, J. Gonzalo, S. Suarez-Garcia, C.N. Afonso, J.P. Barnes, A.K. Petford-Long, R.C. Doole, D.E. Hole: J. Microscopy (Oxford) **201**, 250 (2001)
13 J. Gonzalo, R. Serna, C.N. Afonso, J. Bosbach, T. Wenzel, F. Stietz, F. Träger, D. Babonneau, D. Hole: J. Appl. Phys. **89**, 5734 (2001)
14 E. Borsella, M. Falconieri, S. Botti, S. Martelli, F. Bignoli, L. Costa, S. Grandi, L. Sangaletti, B. Allieri, L. Depero: Mater. Sci. Eng., B **79**, 55 (2001)
15 For example, special issue of Appl. Phys. B **68**(3) (1999)
16 W.C.W. Chan, S.M. Nie: Science **281**, 2016 (1998)
17 M. Bruchez, M. Moronne, P. Gin, S. Weiss, A.P. Alivisatos: Science **281**, 2013 (1998)
18 R. Serna, M.J. de Castro, J.A. Chaos, C.N. Afonso, I. Vickridge: Appl. Phys. Lett. **75**, 4073 (1999)
19 M.J. de Castro, R. Serna, J.A. Chaos, C.N. Afonso, E.R. Hodgson: Nucl. Instrum. Meth. B **166**, 793 (2000)
20 T. Komoda, J. Kelly, F. Cristiano, A. Nejim, P.L. Hemment, K.P. Homewood, R. Gwilliam, J.E. Mynard, B.J. Sealy: Nucl. Instrum. Meth. B **96**, 387 (1995)
21 N. Can, P.D. Townsend, D.E. Hole, H.V. Snelling, J.M. Ballesteros, C.N. Afonso: J. Appl. Phys. **78**, 6737 (1995)
22 T. Shimizu Iwayama, D.E. Hole, P.D. Townsend: J. Luminescence **80**, 235 (1999)
23 T. Shimizu Iwayama, D.E. Hole, I.W. Boyd: J. Phys.: Condens. Matter **11**, 6595 (1999)
24 C.N. Afonso, J. Gonzalo, R. Serna, J.C.G. de Sande, C. Ricolleau, C. Grigis, M. Gandais, D.E. Hole, P.D. Townsend: Appl. Phys. A **69**, S201 (1999)
25 L.R. Doolitle: Nucl. Instrum. Meth. B **9**, 344 (1985)
26 P.D. Townsend, N. Can, P.J. Chandler, B.W. Farmery, R. Lopez-Heredero, A. Peto, L. Salvin, D. Underdown, B. Yang: J. Non-Cryst. Solids **223**, 73 (1998)